Microstructure and residual stress analysis of a 'rim chilled' solid wheel for rail transportation system

G. Donzella[a], S. Granzotto[a], G. Amici[b], A. Ghidini[b], R. Bertelli[b]
[a]*Dipartimento Meccanica - Via Branze, 38 Brescia, Italy*
[b]*Lovere Sidermeccanica S.p.A. - Ricerca & Sviluppo Prodotti e Processi-Lovere (Bg), Italy*

Abstract

The "Rim Chilling" treatment on a railway wheel has been simulated by means of heat transfer and thermal stress fem analyses. Both the microstructure and the residual stress distribution after the chilling have been numerically predicted and verified by means of micrographic observations and strain gauge measurements. A good agreement was found between numerical and experimental results.

Introduction

Some types of railway cars are equipped with braking devices based on shoes acting directly on the tread surfaces of the wheel. Given the considerable thermal stress, the action of the brake shoes aggravates the wear of the wheel, favouring fatigue defects. A differential heat hardening treatment is therefore performed with the purpose of inducing compressive residual stresses in the rim of the wheel, generating conditions capable to oppose the evolution of defects in this way [1]. The term "rim chilling" is justified by the fact that the hardening operation concerns mainly the tread surfaces, whilst the internal part of the wheel (the web and the hub) cools more slowly. In this way high mechanical properties and a residual stress state are obtained in the rim, while the toughness characteristics of the remaining areas are exalted. The correct and repeatable execution of the treatment insures stress levels which correspond to the pre-fixed standards. For this reason it would be advantageous to arrange a calculation model to predict the residual stresses induced by the heat treatment and optimizing the wheel shape [2].

Wheel geometry, material and treatment specification

The shape of the wheel section is reported in fig.1. The rim chilling treatment consists in heating the wheel up to 875°C, placing it in a circular tank where the water can flow only around the rim, mantaining it here for a time of 19 minutes and after that leaving it to cool in calm air. The rim chilling is followed by an tempering at about 515°C for a time of 5 hours. In fig.1 the geometry of the boundary heat exchange during the cooling is also shown. The wheel boundary can be subdivided into three zones with different film conditions: zone A where the material is in contact with running water at 10°C, zone B where the material is in contact with calm air at 20°C and zone C where the material is in contact with air enclosed in cavities or with the asbestos bottom of the tank.

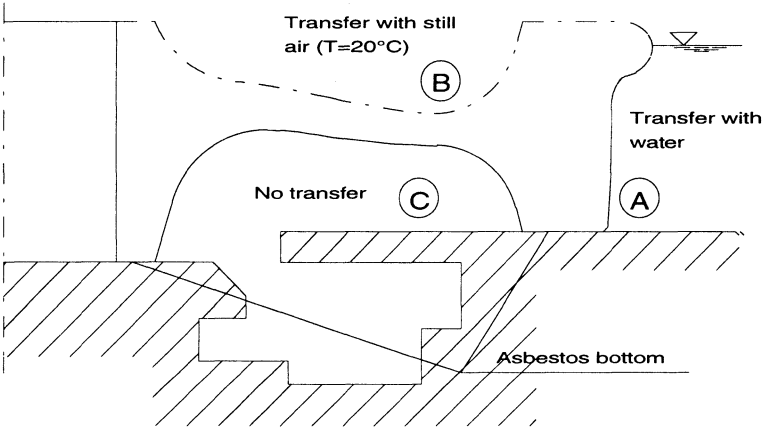

Fig.1: Wheel and treatment apparatus geometry

C	S	P	Mn	Cr	Ni	Mo	Cu	Si	V	Al	Sn	As
0.46	.002	0.01	0.71	0.23	0.12	0.04	0.16	0.34	0.03	.057	.009	.005

Tab.I: Material chemical composition

T [°C]	Conduct. W/m °C	Spec. Heat KJ/Kg °C	σ_Y [MPa] Austenite	σ_Y [MPa] Martensite	σ_Y [MPa] Ferr.-Perl.
20	51.89	486	-	1200	408
200	48.13	515	-	800	318
300	-	-	-	350	286
400	41.85	586	180	-	254
650	34.00	707	65	-	80
900	25.70	623	34.4	-	34.4

Tab.II: Material thermal and mechanical properties as a function of the temperature

The material used for the wheel construction is a R7T U.I.C. 812.3 carbon steel, whose chemical composition is reported in tab.I, while in tab.II the thermal and mechanical properties vs temperature are reported, taken from [3].

Calculation procedure

The numerical calculations were carried out by means of the ABAQUS 5.3 f.e.m. code. The numerical model (fig.2) is composed of 3040 four nodes axisymmetric elements and 3490 nodes. The mesh was strongly refined near the rim, to keep the high thermal and tensional gradient during the cooling.

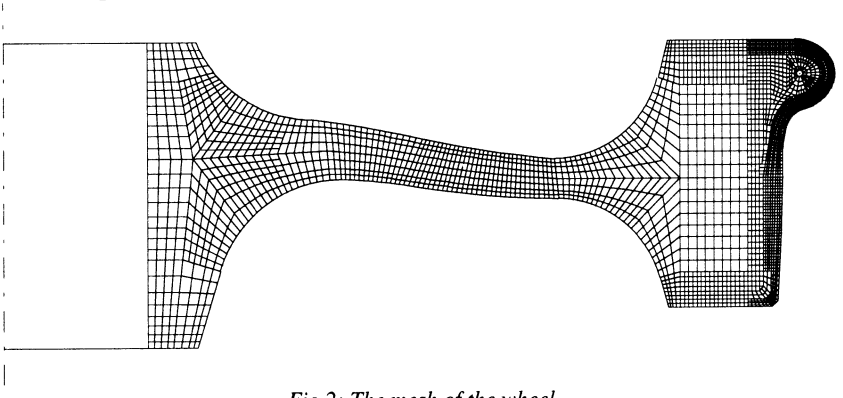

Fig.2: The mesh of the wheel

The analysis is carried out in three subsequent steps (see [4] for a more detailed description):

1) transient heat transfer calculation, in which the temperature distribution in the wheel during the cooling is calculated. The material conductivity and specific heat have been given as a function of the temperature (see table II). The boundary thermal conditions, i.e. the heat transfer coefficient and the radiate coefficient must be carefully specified, to fit the real process. In the time period necessary to move the wheel from the furnace to the chilling tank (about 180 s), the heat transfer coefficient is assumed equal to $35\ W/m^2 \cdot K$ on the whole wheel boundary, which is in contact with calm air at 20°C. During the chilling, the heat transfer coefficient values and, its dependence on the temperature have been given differently in the three zones A, B, C of the wheel surface reported in fig.1:

- in zone A, where the cooling water is present, the typical heat transfer coefficient-temperature diagram [5] shown in fig.3, which takes into account the three stages of the process (formation of a vapour blanket, contact with boiling water, convective heat transfer with calm water) has been assumed;
- in zone B, where the wheel is in contact with open and calm air at 20°C, a heat transfer coefficient value of $35\ W/m^2 \cdot K$, constant with the temperature, has been taken;
- in zone C, where a contact with closed air cavities or with the bottom of the tank is present, the heat transfer coefficient has been taken equal to zero.

The radiate coefficient is important only at high temperature. It has been introduced equal to $5.67 \cdot 10^{-8}\ W/m^2 \cdot K^4$.

2) microstructure prediction, taking into account the phase transformations which happen during the cooling.

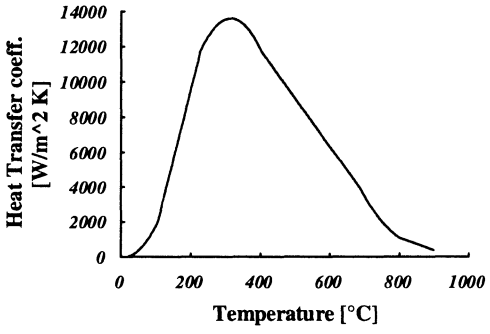

Fig.3: heat transfer coefficient vs temperature

This calculation has been carried out by means of a Turbo Pascal routine which determines the intersection of the cooling curve of each element of the model with the CCT diagram of the material. The result of this step is the microstructure distribution during the cooling and after the chilling. This also makes it possible to define, for each element of the model, the changes of the material mechanical properties as a function of the temperature during the cooling (see table II).

3) thermal stress analysis, carried out taking into account both the thermal history during the cooling, obtained in the first step, and the local changes of the mechanical properties with the temperature obtained from the second step. The expansion coefficient was calculated for each element from the dilatometric curves of the material, experimentally obtained for different cooling rates. The result of this step is the stress and strain distribution during the cooling and after the chilling, i.e. the prediction of the treatment residual stresses in the wheel.

Experimental methods

The experimental verifications concern the temperature distribution during the cooling, the microstructure distribution and the residual stress state after the rim chilling. The temperature measurements were carried out by means of two thermocouples and a portable pyrometer, respectively in the points T1, T2 and P1, P2 shown in fig.4. The microstructure distribution was verified by means of SEM observations in the points near the rim (see fig.8).

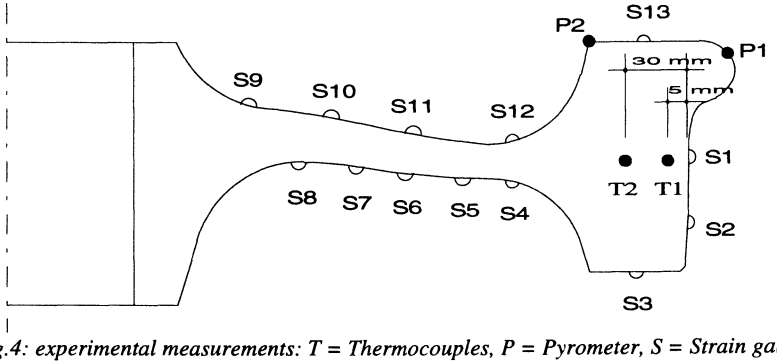

Fig.4: experimental measurements: T = Thermocouples, P = Pyrometer, S = Strain gauges

The hoop residual stresses were measured by means of the strain gauges S1 to S13, cutting a sector of the wheel and calculating the differences from the measurements taken after and before the cutting.

Microstructure analysis

In fig.5 the temperature distribution in the wheel in the initial stage of the cooling is shown. The high thermal gradient near the rim in this stage can be noted from this figure.

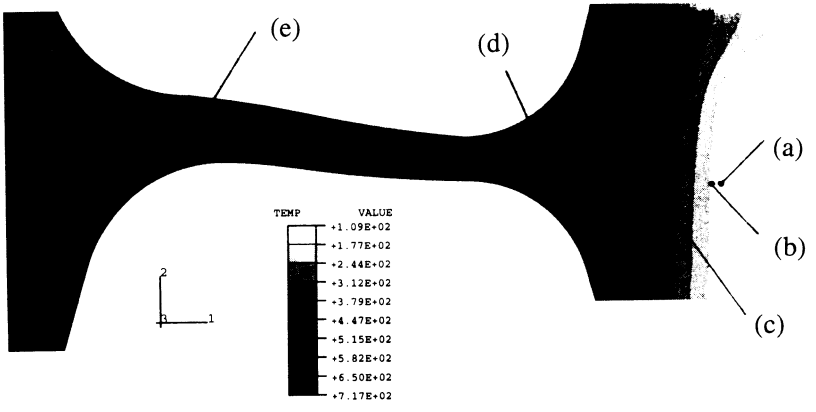

Fig.5: Temperature distribution at the beginning of the chilling

The numerical prediction of the temperature distribution during the cooling has been verified by means of the two thermocouples and the portable pyrometer. The comparison between experimental and numerical cooling curves is reported in figs.6a and 6b, for thermocouples and pyrometer, respectively. A good agreement can be noted from this figure.

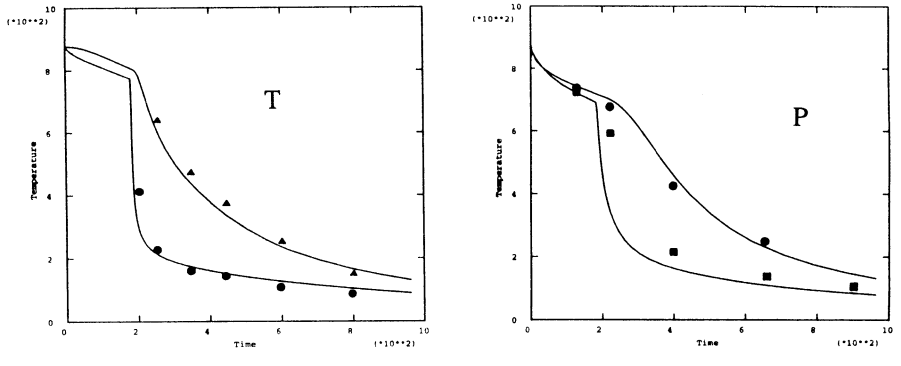

(a) *(b)*

Fig.6: Numerical and experimental cooling curves

The cooling curves of the most representative nodes of the model (shown in fig.5) are reported in fig.7 with the CCT diagram of the material.

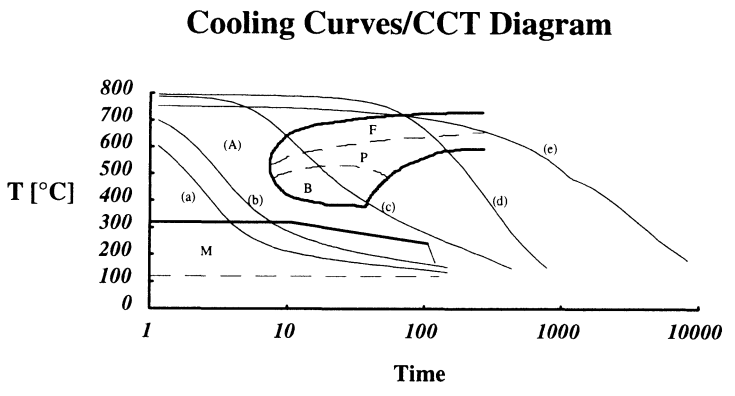

Fig.7: Numerical cooling curves and CCT diagram of the material

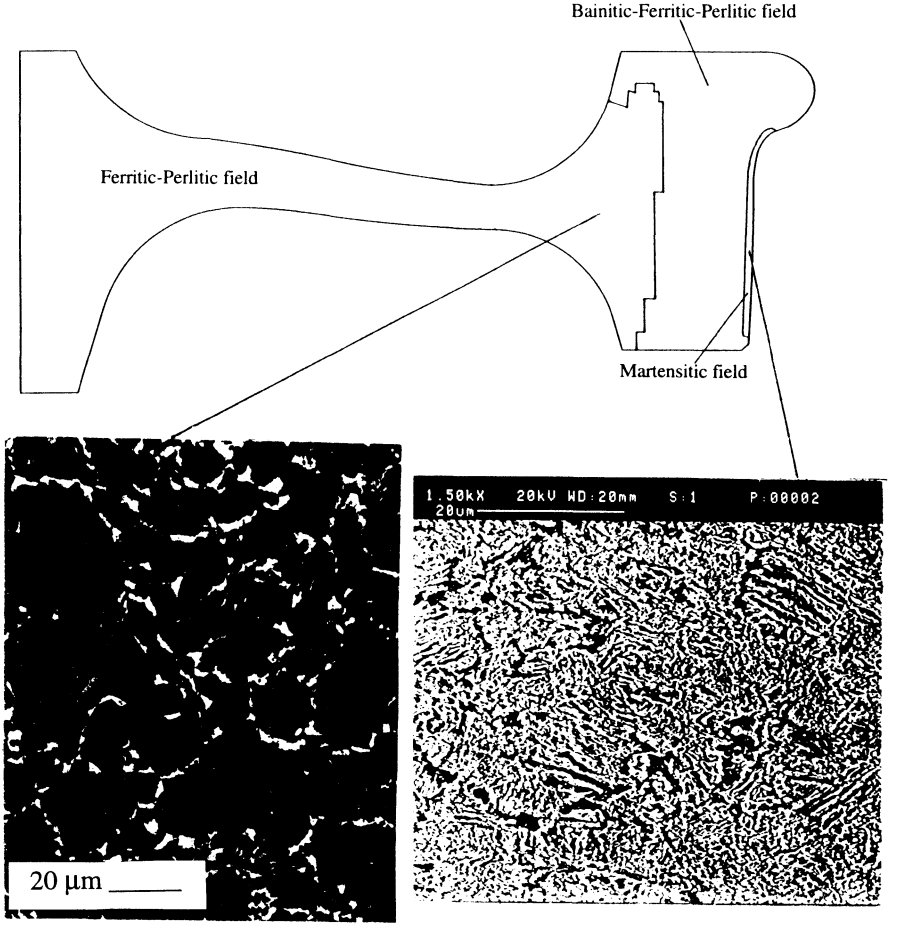

Fig.8: Microstructure map after chilling and micrographs after chilling and tempering

It can be observed from this figure that the martensitic transformation happens only in the zone very close to the rim surface, while most of the wheel is in a ferritic-pearlitic state at the end of the treatment. A transition zone with a ferritic-pearlitic structure and traces of bainite can also be observed in proximity of the wheel surface. This prediction is well shown by the numerical microstructure map after the chilling reported in fig.8, where a surface martensite layer of about 3 mm is clearly notable. The experimental micrographic observations carried out in two points near the rim confirm these results.

Residual stress analysis

The deformed mesh of the wheel and the hoop residual stress distribution after the chilling is shown in fig.9. A strong compressive area near the rim and an evident bending effect on the slim web can be noted.

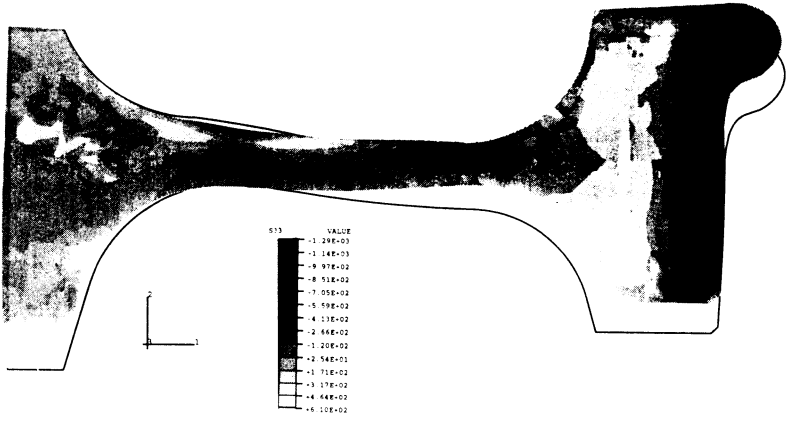

Fig.9: Deformed mesh and hoop residual stress contour after the chilling

The numerical residual stress distribution is confirmed by the strain gauges measurements reported in tab.III.

Strain gauges	Numerical [MPa]	Exp. [MPa]	Strain gauges	Numerical [MPa]	Exp. [MPa]
S1	-868	-693	S8	243	199
S2	-595	-742	S9	-10	6
S3	-470	-400	S10	-280	-131
S4	292	300	S11	125	-25
S5	363	332	S12	270	305
S6	444	409	S13	-472	-302
S7	350	349			

Tab.III: Numerical and experimental hoop residual stresses

Conclusions

The transient heat transfer analysis has been successfully carried out taking carefully into account the thermal boundary conditions and the different heat transfer stages during the cooling. The dependence of the heat transfer coefficient on the temperature was in particular decisive in determining the correct cooling curves of the model, verified by the experimental measurements. The microstructural changes which happen during the treatment have been predicted intersecting the numerical cooling curves with the CCT diagram of the material, by means of a Turbo Pascal routine. This has also made it possible to assign the correct material mechanical and thermal properties to each point of the model, as a function of the temperature. The numerical prediction of the microstructure distribution after the rim chilling has shown a martensitic layer of about 3 mm near the rim surface, confirmed by SEM observations.
The thermal stress analysis has been carried out on the basis of the cooling curves and the correspondent changes in the material properties, calculated in the previous steps. The numerical prediction of the residual stress state after the rim chilling has shown a strong compressive zone near the rim surface and a bending effect on the web. This has been confirmed by the strain gauges measurements.

References

1. Amici G., Vanolo P., Bianchi C., *The development of a new generation of railway wheels*, WCRR International Congress, Paris, November 1994.
2. Diener M., Müller R., Ghidini A., Scepi M., *Study on fracture toughness of R7T UIC 812.3 steel solid wheels applying traditional and innovative fracture mechanics parameters*, X International Wheelset Congress, Sidney, September 1992.
3. Colin J. Smithells, *Metal Reference Book*, Vol.II, Butterworths, London, 1962.
4. Donzella G., Granzotto S., *Numerical Investigation of the Microstructure and Residual Stress Prediction of a Quenched Steel Cylinder*, Proceedings of the 5° National Congress of the Abaqus Users' Group Italia, Milan, 26-27 september, 1994.
5. Liscic B., Tensi H.M., Luty W., *Theory and Technology of Quenching*, Springer-Verlag Berlin, Heidelberg, 1992.